Evaluation of infection risk of two endoparasites to moose (Alces alces) in the Adirondack Park of New York

Alec Wong[1], Krysten Schuler[1], Angela Fuller[1,2,3]

[1]Cornell University
[2]New York Cooperative Fish and Wildlife Research Unit
[3]U.S. Geological Survey

Abstract

Endoparasites *Parelaphastrongylus tenuis* and *Fascioloides magna* were attributed to 19% and 21% of mortalities in New York in 2015, respectively, and may be contributing factors to limiting moose (*Alces alces*) populations in the Adirondacks region. Field surveys were conducted to collect white-tailed deer (*Odocoileus virginianus*) fecal pellets under distance sampling protocol both to measure relative deer density and to diagnose the infection status of the pellets by *P. tenuis* and *F. magna*. Over the three years of data collection, 41.7% of fecal pellets collected ($N = 656$) contained *F. magna* eggs, and 34.7% of fecal pellets contained L1 *P. tenuis* larvae. We attempted to quantify the geospatial distribution of parasite infection using landscape variables such as habitat, geomorphon structure, elevation, and spatial trend, but goodness-of-fit tests indicated poor fit of the model structures we evaluated, whether assessed as continuous intensity of infection (Poisson, negative binomial), or binary infection status (binomial). We conclude that the data are not extensive enough to quantify relationships between parasite infection in white-tailed deer fecal pellets and geospatial effects.

Introduction

Moose (*Alces alces*) populations are in decline in parts of their range in North America such as in Minnesota, Vermont, and New Hampshire in the United States of America and Nova Scotia, Alberta, Saskatchewan, Manitoba, and Ontario in Canada (Lankester 2018; Timmermann and Rodgers 2017). Some researchers point to parasite infection from liver fluke (*Fascioloides magna*) and/or brainworm (*Parelaphastrongylus tenuis*) as contributing factors to these declines (Murray et al. 2006; Lankester 2010, 2018; Wünschmann et al. 2015), although this claim is controversial (Lenarz 2009) and in some areas may coincide with other factors such as depredation or low reproduction rates that may disguise effects of parasite infection (Barber-Meyer and David Mech 2016; Kuzyk et al. 2018). Nevertheless, brain worm and liver fluke cause morbidity and mortality in moose populations and should be monitored.

Infections by *P. tenuis* are benign to white-tailed deer (*Odocoileus virginianus*), but cause severe neurological disorders in moose caused by migration of larvae through the central nervous system that often end in death (Pybus 2001; Lankester 2010). *Parelaphastrongylus tenuis* is acquired via ingestion of gastropod intermediate hosts, in which *P. tenuis* larvae have molt from L1 to L2, and L3 stages over approximately 4 weeks. Gastropods become infected by ingesting the mucuosal layer surrounding white-tailed deer fecal pellets, or from the soil over which the L1-stage larvae have been washed by precipitation.

Fascioloides magna infection damage manifests as lesions in the hepatic tissue due to migration of immature flukes or fibrous encapsulation of adult flukes (Pybus 2001). Again, moose are thought to become infected through ingestion of gastropod intermediate hosts. A major distinction is that the gastropod hosts are aquatic snails (typically within the genus *Lymnaea*) that become infected by free-swimming miracidia introduced to the water as eggs in white-tailed deer feces (Pybus 2001; Peterson et al. 2013; Malcicka 2015). The meracidia develop within the snail, ultimately generating cercariae that encyst as metacercariae on aquatic vegetation. Because moose select aquatic vegetation as a significant proportion of their diet, *F. magna* metacercariae are presumably commonly consumed by moose.

In the Adirondacks of New York, moose populations have increased since their extirpation in the late 19th century, but their populations have not seen the same growth during the 20th century as their New England counterparts (Timmermann and Rodgers 2017). Recent estimates of moose population size indicate that there are approximately 600 to 1000 moose in the Adirondacks (Wong, Fuller, and Royle, n.d.), a range which does not indicate substantial change from previous assertions of population size (Hickey 2008). Factors that may be limiting the population are not established, but the focal parasites *P. tenuis* and *F. magna* have been observed in moose necropsies with moderate frequency (REF Schuler and/or DEC).

The New York State Department of Environmental Conservation (DEC) has been gathering information on moose health from incidental mortalities (n = 117) since 2000 and the Animal Health Diagnostic Center (AHDC) started live moose testing in 2015. Moose in New York State appear to be substantially impacted

by several parasites excepting winter ticks, which are more common in New England states. Over 19% of mortalities were attributed to P. tenuis, 21% of moose carcasses examined were infected with liver flukes (Fascioloides magna). Migrating parasites cannot be detected in live moose, but were likely a problem as New York moose had 5-6x higher eosinophil (white blood cell) counts than New Hampshire or Maine moose.

The geospatial distribution of infection risk to moose is a concern for management, and we attempt to quantify this by first assessing the spatial patterns in infection of white-tailed deer fecal matter.

Materials and Methods

Study area

We surveyed within the Adirondack Park of the state of New York. It is an area of approximately 24,000 km^2, composing approximately 17% of the state of New York. Elevation ranges from 100m - 1600m. The Adirondack Park contains primarily upland forest habitat dominated by such species as American beech (*Fagus grandifolia*), red spruce (*Picea rubens*), hemlock (*Tsuga canadensis*), sugar maple (*Acer saccharum*), striped maple (*Acer pensylvanicum*), and balsam fir (*Abies balsamea*). Approximately 20% of the park is composed of wetland habitats including open river corridors, floating bogs, and large open bogs dominated by conifers (Hickey 2008).

Field data collection

White-tailed deer fecal pellet groups were collected opportunistically during the years of 2016 and 2017 for the purpose of parasite quantification during a larger survey investigating the population size of moose in the park. The moose study surveyed triangular transects approximately 3 km long, selected by cluster random sampling. The clustering design of the transects were optimized for a spatial capture-recapture survey, including 3 transects per cluster separated by approximately 2-4 km.
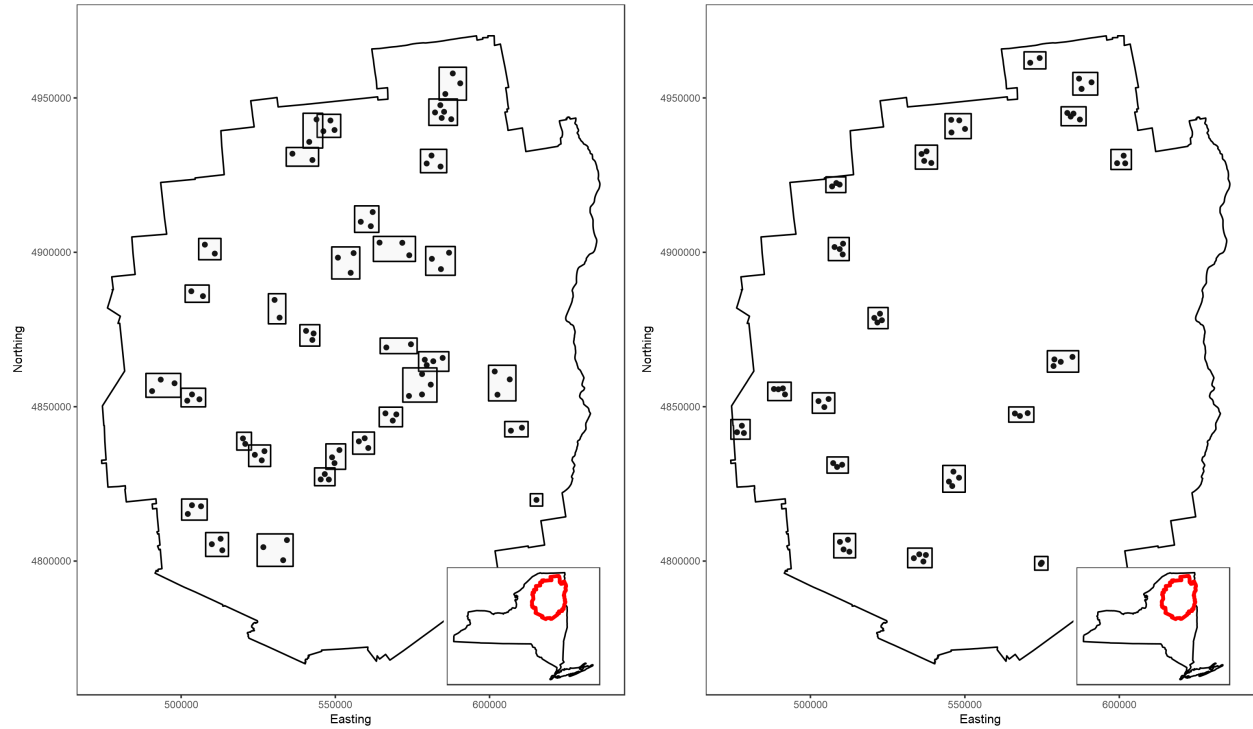
(a) Transect locations within the Adirondack Park for the 2016 survey.

(b) Transect locations within the Adirondack Park for the 2017 survey.

Figure 1: Transect locations within the Adirondack Park for the 2017 survey. Each dot represents the location of one transect, and each cluster of transects is bounded by a box. The inlaid plot indicates the extent of the Adirondack Park relative to the state of New York.

In 2018, a single-observer distance sampling protocol was implemented to quantify deer fecal group abundance in addition to measuring parasite intensity. Along each moose transects, 6 distance sampling transects each 100m long were spaced 200m apart from each other. **INSERT FIGURE FOR DEER TRANSECTS** A total of 150 transects were sampled in 2018. At the specified start point, field technicians extended a 100m tape to serve as the center line, and made observations along its length. Any number of scat pellets were considered to constitute a fecal group, and the approximate number was recorded. When a fecal group was detected, its distance perpendicular from the center line, and parallel along the center line was recorded. The perpendicular distance is the focal variable of distance sampling, but the parallel distance provided highly precise location coordinates of the scats – because the start point of the transect was recorded with greater accuracy (due to longer GPS averaging time), the coordinates of the scats could be refined by translating the start point in space by the angle of the transect, and the parallel distance away from the start point.

Fifty-seven white-tailed deer fecal samples were collected in 2016, 391 samples were collected in 2017, and 174 samples were collected in 2018.

Parasitological analyses

The fecal samples were analyzed by the Cornell Animal Health and Diagnostic Center using several methods. For *F. magna*, Flukefinder, a modified Baermann technique, and fecal quantitative flotation were used. For *P. tenuis*, the modified Baermann, and fecal quantitative flotation methods were implemented. After 2016, the performant method for *F. magna* was determined to be Flukefinder, and for *P. tenuis* the performant method was the modified Baermann technique. This was assessed by **HOW? ASK KRYSTEN**, and validated post-hoc to have the greatest detection probability by an occupancy analysis.

Flukefinder

Needs to be updated by relevant members; Flukefinder methodology not in shared folder

Modified Baermann

Fecal flotation

Statistical Models

For analysis of relative risk of infection to moose, we implemented a hierarchical Bayesian modeling framework analyzed with the `R` package `INLA`, which uses integrated nested Laplace approximation to approximate the posterior distribution of model parameters.

Parasite intensity model

Let $\widehat{\lambda}(s)$ be the estimated per-fecal-group-sample abundance (or, intensity in the epidemiological sense). Let $S = \{s_i, i = 1, ..., n\} \subset \Omega$ be the n distinct locations where white-tailed deer fecal groups were observed within the observation region $\Omega \subseteq \mathbb{R}^2$, and let y_i be the observed parasite count within the fecal sample.

Parasites observed within each scat sample are ≥ 0, and due to the high prevalence of 0's, we considered a negative binomial distribution for the response in addition to the Poisson. On any bounded region $B \subseteq \Omega$, observations are thus modeled as follows:

$$y_i \sim \text{Poisson}(\mu_i)$$
$$\log(\mu_i) = \beta_0 + \beta_1 * x_1(s_i) + ... + \beta_p * x_p(s_i) + \Psi_1(s_i) \tag{1}$$
$$\Psi_1(s_i) \sim GP(0, \Sigma)$$

Where, y_i represent the parasites observed per fecal group sample, μ_i is the mean function modeled dependent upon spatial covariates $x_j(s)$, and $\Psi_1(s)$ is a Gaussian process with mean 0 and covariance matrix Σ. The covariance function used is the Matern; with $\nu = \alpha - d/2$, and $\alpha = 2; d = 2$:

$$\text{cov}[\Psi(s), \Psi(s')] = \sigma_\Psi^2 \ \kappa||s' - s|| \ \mathcal{K}_1(\kappa||s' - s||)$$

where τ, κ are variance and range scaling parameters, respectively, $\sigma_\Psi^2 = 1/(4\pi\kappa^2\tau^2)$ is the marginal variance, and $\mathcal{K}_1$ is the modified Bessel function of the second kind and order 1 (See Lindgren and Rue (2015) for the specific representation and estimation of the spatial random effects within INLA). We selected this error model to account for the fact that the spatially clustered sampling is likely to obtain multiple samples from the same individuals, inducing local spatial autocorrelation. While empirical variograms do not demonstrate autocorrelation at any distance for *F. magna* response values, there exists observed autocorrelation for *P. tenuis* at the scale of approximately 1200 m.

Additionally, we assessed the fit of models treating the response as a binary random variable modeled under the binomial distribution and zero-inflated binomial distribution, with the same model of spatial dependence instead using the appropriate link function.

Covariates on parasite intensity

In our model, we consider the following covariate effects on parasite intensity. Coordinate data (UTM Easting and Northing) are included to model broad-scale spatial trend. We considered a derived variable of precipitation representing the total accumulation of precipitation in the year prior to the data collection date, measured in inches. Precipitation affects the survival of *P. tenuis* and *F. magna* outside of a host (i.e. as L1

larvae, and eggs in feces, respectively), and so it is anticipated that deer would be more likely to be infected in areas of higher rainfall (Pybus 2001). Additionally, gastropod activity is inhibited by drought, and so higher rainfall would suggest higher risk of infection due to a greater availability of gastropods to be ingested in the case of *P. tenuis* (Lankester 2018). We used the spatially interpolated PRISM dataset for precipitation (n.d.). We considered another derived variable for snowfall accumulation in the snowfall season prior to the data collection date (that is, from September until April prior to the date of survey). Similar to precipitation, we anticipate that areas that experience low snowfall in the year prior to the survey date will exhibit a higher parasite intensity due to increased parasite survival, and increased activity of gastropod intermediate hosts. The National Weather Service's National Snowfall Analysis dataset was used to obtain spatially-referenced snowfall amounts.

Local terrain basins where water may collect were considered as a potentially important effect particularly for *F. magna*, as the life cycle of the parasite has a period during which metacercariae encyst on aquatic vegetation and once matured infect aquatic snail intermediate hosts. We hypothesized that intensity of infection for *F. magna* will be greater in basins than on slopes or peaks, and we assessed this by the geomorphon tool in QGIS, assessed at a resolution of 40km (1600 squared-kilometers). This resolution was selected because it maximized the variation in the geomorphon classification distribution relative to our sample locations.

INLA settings

Priors

We used default priors set by INLA for the covariate coefficients; that is:

$$\beta_p \sim \text{Normal}(0, 0.001)$$

where the second argument of the Normal distribution is specified on the *precision* scale.

The priors for the Matern covariance parameters were specified using INLA's penalized complexity prior construction for the spatial range parameter ρ and marginal standard deviation σ_0. The joint density of the prior is:

$$p(\rho, \sigma_0) = \frac{(d * R * S)}{2} \rho^{-1-\frac{d}{2}} \exp(-R\rho^{\frac{-d}{2}}) \exp(-S\sigma_0)$$
$$R = -\log(p_\rho)\rho_0^{\frac{d}{2}} \tag{2}$$
$$S = -\frac{\log(p_\sigma)}{\sigma_0}$$

Critically, p_ρ and p_σ are defined such that:

$$p_\rho = P(\rho < \rho_0)$$
$$p_\sigma = P(\sigma > \sigma_0)$$

In so doing, the prior specification can be defined on intuitive scales, setting a lower and upper limit for ρ and σ_0, respectively. We selected $\rho_0 = 100$ (meters) and $\sigma_0 = 1$, and $p_\rho = p_\sigma = 0.01$ reasoning that spatial autocorrelation < 100m is indistinguishable from white noise, and the marginal standard deviation would not be much larger than the sample standard deviation.

Mesh

A mesh is required to fit Gaussian random effect models under the INLA framework. The `meshbuilder` tool provided by package `INLA` was used to visually select settings that fulfilled the following criteria (see Figure 2):
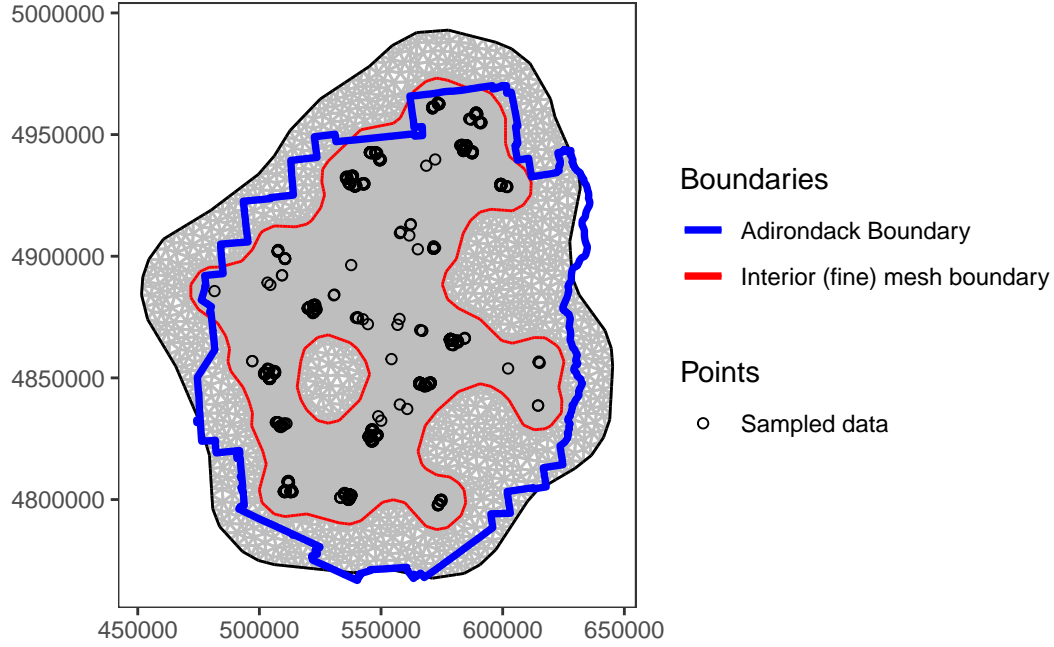
Figure 2: Boundary line of the Adirondack Park (blue), and the mesh constructed for INLA (red).

- Relatively fine mesh resolution (< 1km) in the vicinity of sampled data
- Relatively low mesh resolution far from sampled data (>5km)

Model Specifications

Six models were applied using the covariates developed above upon response variables for both *F. magna* and *P. tenuis.*

Table 1: Model specifications and their covariates

Model	Formula
Null Model	.
Full Model	Easting + Northing + Precipitation + Snow + Geomorphon + Elevation + Gaussian Process (GP)
Fixed Effects Model	Easting + Northing + Precipitation + Snow + Geomorphon + Elevation
Fixed Effects Parasite Survival Model	Precipitation + Snow + Geomorphon
Two-scale spatial model	Easting + Northing + GP
Two-scale spatial model and elevation	Easting + Northing + Elevation + GP

Results

We observed 41.7% positive diagnoses of *F. magna* over the three years of data collection ($N = 656$), with yearly positive results being 69% in 2016, ($N = 80$), 37.8% in 2017 ($N = 402$), and 38.5% in 2018 ($N = 174$). For *P. tenuis* we observed 34.6% infection prevalence among the fecal samples tested over all three years, with yearly positive results being 48.8% in 2016 ($N = 80$), 23.9% in 2017 ($N = 402$), and 52.6% in 2018 ($N = 174$) (Table 2).

Table 2: Raw frequencies and proportions of diagnoses performed on white-tailed deer fecal samples between 2016 and 2018.

Diagnosis	Species	Counts 2016	2017	2018	Proportions 2016	2017	2018
Positive	F. magna	55	152	67	0.688	0.378	0.385
	P. tenuis	39	95	92	0.488	0.239	0.526
Negative	F. magna	25	250	107	0.312	0.622	0.615
	P. tenuis	41	302	83	0.512	0.761	0.474

Model results

Model comparison was implemented by comparison of WAIC values produced by INLA. This information criterion is a measure of *relative* out-of-sample predictive accuracy, and lower WAIC values indicate greater relative performance.

Model results for the Poisson response distribution are not included in the table because all AIC values are an order of magnitude larger than those of the negative-binomial response distribution.

F. magna

Among the models fit to the *F. magna* data, the best-supported model was the global model, followed by the second-best model with a delta-WAIC value of 24.41.

Model Name	WAIC
Full model	3052.46
Two-scale spatial model	3076.87
Two-scale spatial model and elevation	3081.90
Fixed effects model	3108.38
Fixed Effects Parasite Survival Model	3110.83
Null Model	3130.45

P. tenuis

Among the models fit to the *P. tenuis* data, the best-supported model was the reduced 'two-scale spatial model', which had only easting, northing, and the Gaussian process error model. The next best performing model followed with a delta-WAIC value of 7.06.

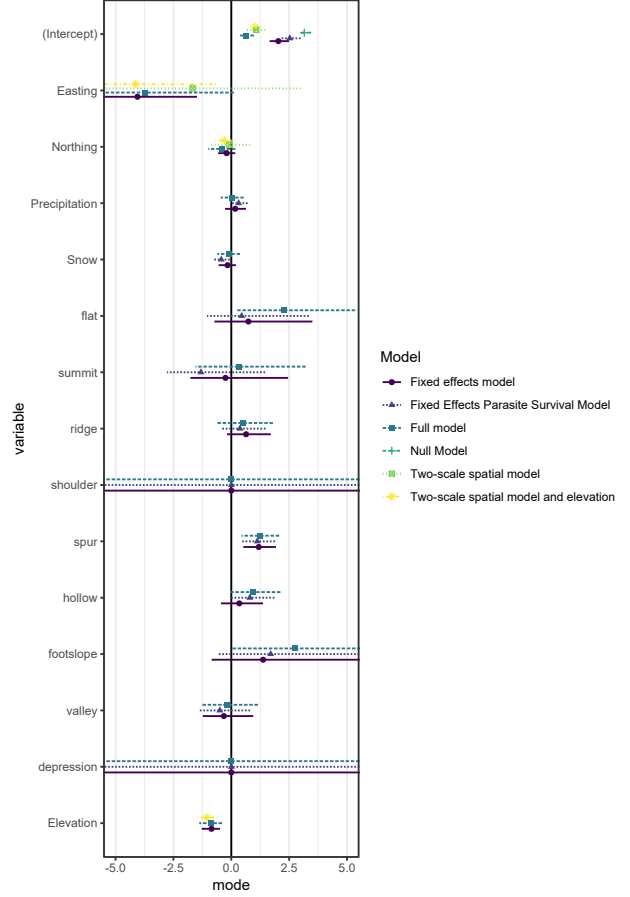| Model Name	WAIC
Two-scale spatial model	2756.66
Full model	2763.73
Two-scale spatial model and elevation	2767.49
Fixed effects model	2795.65
Fixed Effects Parasite Survival Model	2823.91
Null Model	2824.85

Fixed effects parameter estimates

Most parameters either covered 0
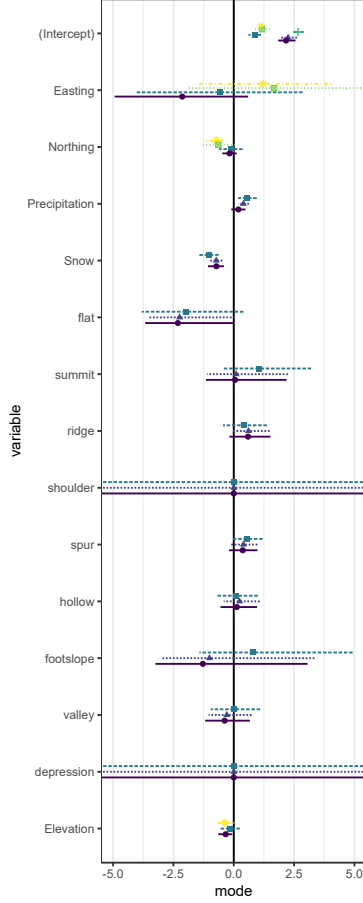
(a) *F. magna* model parameter estimates.

(b) *P. tenuis* model parameter estimates.

Figure 3: Displayed are the mode and 95% credible interval for coefficients of fixed effects. See Appendix A for exact values.

Bayesian model checks

We checked the fit of the models using Bayesian predictive checks made available by the `INLA` package; specifically the conditional predictive ordinate (CPO) and the probability integral transform (PIT).

Conditional predictive ordinate

The conditional predictive ordinate (CPO) is a leave-one-out cross-validation measure, defined as

$$\mathrm{CPO}_i = \pi(y_i^{\mathrm{obs}}|y_{-i})$$

and describes the probability of observing of a particular observation when all of the data but observation i are used to fit to the model. Very small values indicate that the model is not likely to have predicted a particular observation and thus that model is not expected to generalize well.

All of our models exhibited poor performance with roughly half of the data points having low CPO values less than 0.1 (Figure 4). In addition, the data points with low CPO values are strongly related to those

points with the response > 0 (Figure 6). This indicates that the models overall fit the data poorly, having almost no predictive power to the domain of the response of interest.
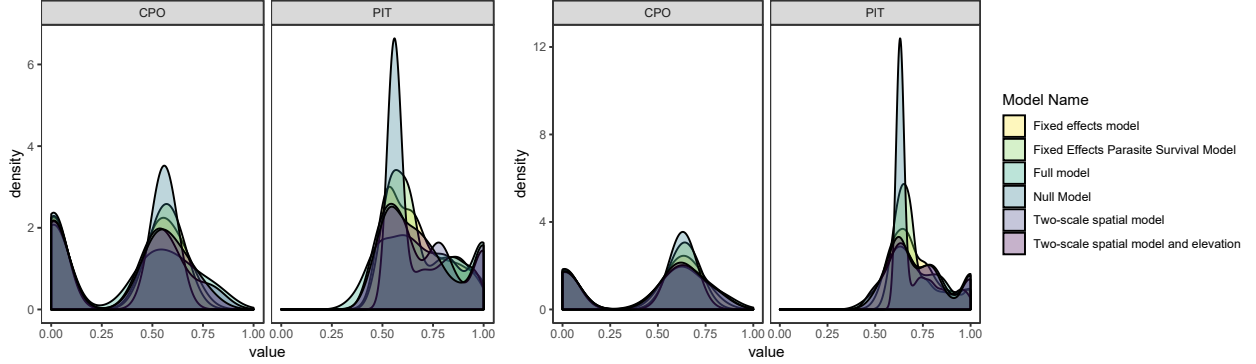
(a) *F. magna* model goodness-of-fit statistics.

(b) *P. tenuis* model goodness-of-fit statistics.

Figure 4: Displayed are the densities of two goodness-of-fit statistics for the models applied to the two parasite species' data. Under good model fit, the CPO values should not have many values approaching zero; the PIT values should be uniformly distributed.

Probability integral transform

Another goodness-of-fit measure that `INLA` provides is the probability integral transform value (PIT), which measures the probability of predicting a new observation less than or equal to the observed data value. More generally the probability integral transform states that the cumulative distribution function $\mathcal{F}$ of a random variable X evaluated at x_i for all i will have a random uniform distribution if the random values x_i are indeed generated by the same process as X. If we take $\mathcal{F}(X)$ to be predictions from a fitted model, departure from uniformity indicates that the observations x_i may not be well predicted by the model.
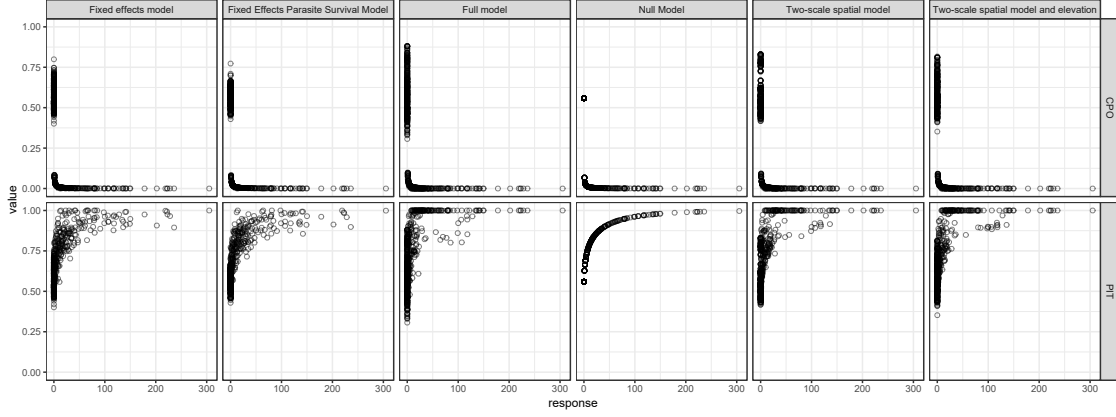
(a) *F. magna* model goodness-of-fit statistics.
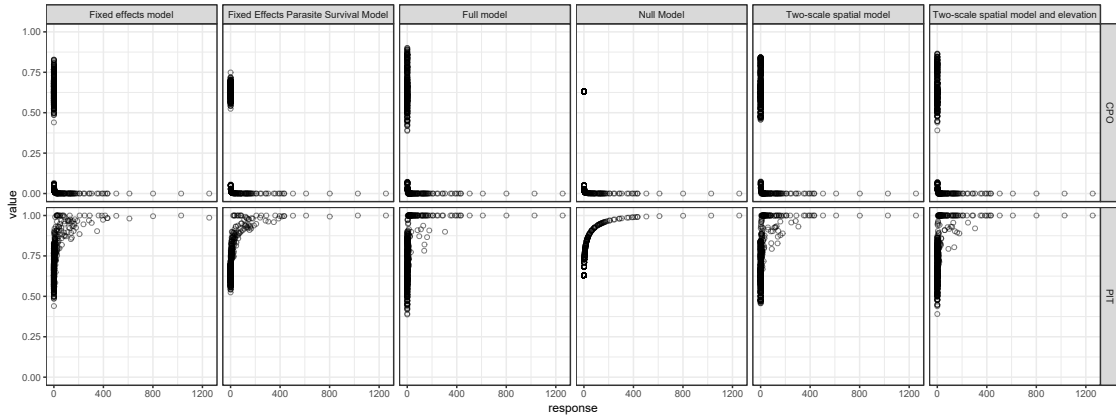
(b) *P. tenuis* model goodness-of-fit statistics.

Figure 5: Displayed are the conditional predictive ordinate and probbability transform values across values of the response variable. The goodness-of-fit values are relatively poor when the response is not zero.

By visual assessment, the PIT values are not uniformly distributed (Figure 4), and become more concentrated around 1 with increasing values of the response (Figure 6).

Binary model results

Due to the poor fit, the models were reassessed with the data converted to binary presence-absence data, and the best-performing models by WAIC were re-assessed. The conditional predictive ordinate values were improved, having few values below 0.1. However, the probability integral transform continued to indicate a lack of fit, having a high density of values approaching unity.
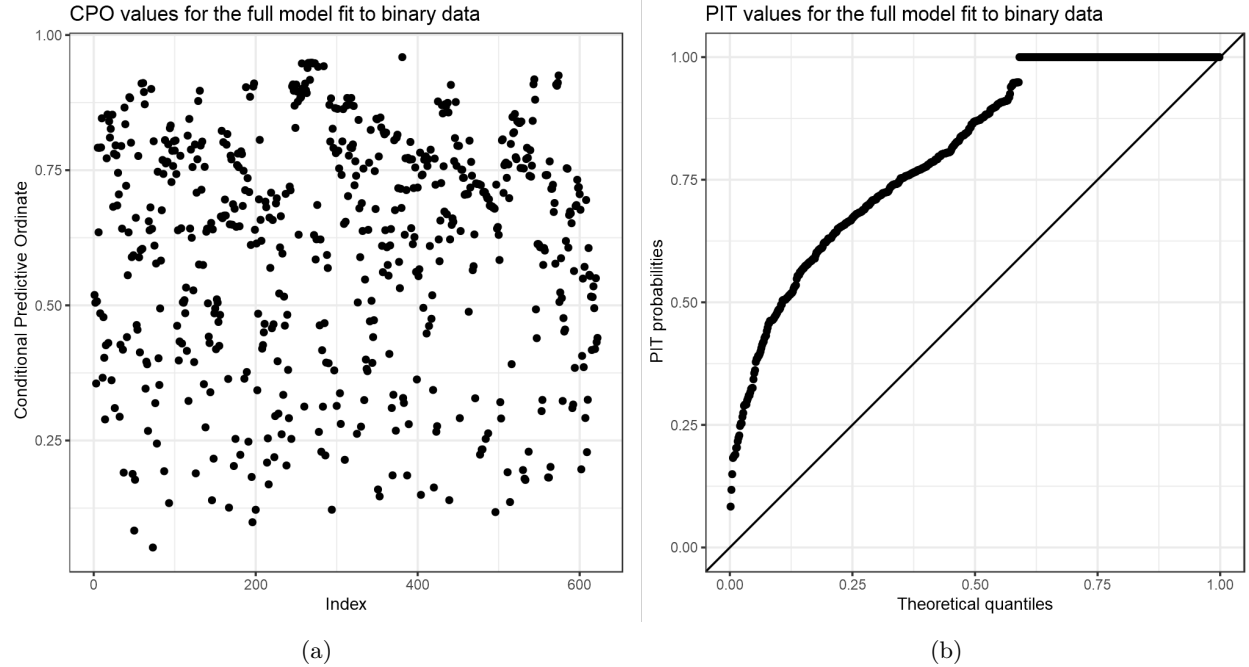
Figure 6: Displayed are the (a) conditional predictive ordinate and (b) probability transform values.

Discussion

The endoparasites *F. magna* and *P. tenuis* are moderately prevalent in the Adirondack white-tailed deer population, having infected approximately four-in-ten of the deer pellet groups assessed for both parasites. This should not be interpreted as an assessment of the white-tailed deer population, as it is possible that we resampled individuals' pellet groups; nevertheless, a relatively abundant population of infected pellet groups will present a higher risk of infection to gastropod intermediate hosts, and so there is no

The best-performing model fit to the *F. magna* data indicate a small negative effect of UTM Northing, and each model including Snow as a covariate demonstrate a

However, our analysis of factors explaining the spatial distribution of the parasites are inconclusive due to poor model fit. Two goodness-of-fit measures indicate that all model constructions have poor fit, particularly for response values far from zero. This indicates two things: (a) the selection of the random field parameters are not contributing to the lack of fit (as the models without local spatial effects exhibit the same fit statistics), and (b) the model does not explain the parasite presence very well at all.

While the negative binomial model presents a tremendous improvement over the Poisson, the overall lack of fit indicates that a different analytical framework is required. The poor fit persisted even when the data were reduced to presence/absence binary information. The spatial covariates included are likely not adequate in explaining the variation, and the data are likely too sparse to present a signal over as large a space as the Adirondacks.

References

Barber-Meyer, Shannon, and L. David Mech. 2016. "White-tailed Deer (Odocoileus virginianus) Subsidize Gray Wolves (Canis lupus) During a Moose (Alces americanus) Decline: A Case of Apparent Competition?" *Canadian Field-Naturalist* 130 (4): 308–14. https://doi.org/10.1016/j.tig.2014.09.010.

Hickey, Lisa. 2008. "Assessing re-colonization of moose in New York with HSI models." *Alces* 44 (44): 117–26.

Kuzyk, Gerald, Ian Hatter, Shelley Marshall, Chris Procter, Becky Cadsand, Daniel Lirette, Heidi Schindler, et al. 2018. "Moose Population Dynamics During 20 Years of Declining Harvest in British Columbia." *Alces* 54: 101–19.

Lankester, Murray W. 2018. "Considering weather-enhanced transmission of meningeal worm, Parelaphostrongylus tenuis, and moose declines." *Alces: A Journal Devoted to the Biology and Management of Moose* 54: 1–13. http://alcesjournal.org/index.php/alces/article/view/201.

Lankester, Murray W. 2010. "Understanding the impact of meningeal worm, Parelaphostrongylus tenuis, on moose populations." *Alces* 46: 53–70.

Lenarz, Mark S. 2009. "A review of the ecology of Paralephostrongylus tenuis in relation to deer and moose in North America." *Summaries of Wildlife Research Findings*, no. Benson 1958: 1–7.

Lindgren, Finn, and Håvard Rue. 2015. "Bayesian Spatial Modelling with R - INLA." *Journal of Statistical Software* 63 (19). https://doi.org/10.18637/jss.v063.i19.

Malcicka, Miriama. 2015. "Life history and biology of fascioloides magna (Trematoda) and its native and exotic hosts." *Ecology and Evolution* 5 (7): 1381–97. https://doi.org/10.1002/ece3.1414.

Murray, Dennis L, Eric W Cox, Warren B Ballard, Heather A Whitlaw, Mark S Lenarz, Thomas W Custer, Terri Barnett, and Todd K Fuller. 2006. "Pathogens, nutritional deficiency, and climate influences on a declining moose population." *Wildlife Monographs* 166 (Murray): 1–30. https://doi.org/10.2193/0084-0173(2006)166[1:PNDACI]2.0.CO;2.

Peterson, William J., Murray W. Lankester, John G. Kie, and R. Terry Bowyer. 2013. "Geospatial analysis of giant liver flukes among moose: Effects of white-tailed deer." *Acta Theriologica* 58 (4): 359–65. https://doi.org/10.1007/s13364-013-0130-4.

Pybus, Margo. 2001. *Parasitic Diseases of Wild Mammals.* Edited by William M. Samuel, Margo J. Pybus, and A. Alan Kocan. Ames, Iowa: Iowa State University Press. https://doi.org/10.2307/1295958.

Timmermann, H R, and Arthur R Rodgers. 2017. "The status and management of moose in North America - Circa 2015." *Alces* 53: 1–22.

Wong, Alec, Angela Fuller, and J. Andrew Royle. n.d. "Quantification of Moose (Alces Alces) Population from Scat Counts Made by Detection Dogs."

Wünschmann, Arno, Anibal G. Armien, Erika Butler, Mike Schrage, Bert Stromberg, Jeff B. Bender, Anna M. Firshman, and Michelle Carstensen. 2015. "Necropsy findings in 62 opportunistically collected free-ranging moose (Alces alces) from Minnesota, USA (2003–13)." *Journal of Wildlife Diseases* 51 (1): 157–65. https://doi.org/10.7589/2014-02-037.

n.d. Oregon State University; PRISM Climate Group; http://prism.oregonstate.edu.

Appendices

Appendix A: Parameter estimates for the negative binomial model

Table 3: Fixed effect parameter estimates and distribution for *F. magna*

variable	mean	sd	0.025quant	0.5quant	0.975quant	mode
Null Model						
(Intercept)	2.670	0.116	2.450	2.668	2.905	2.663
Full model						

Table 3: Fixed effect parameter estimates and distribution for *F. magna (continued)*

variable	mean	sd	0.025quant	0.5quant	0.975quant	mode
(Intercept)	0.871	0.132	0.610	0.871	1.129	0.872
Easting	-0.573	1.750	-4.028	-0.568	2.854	-0.559
Northing	-0.122	0.247	-0.604	-0.123	0.367	-0.125
Precipitation	0.560	0.197	0.179	0.559	0.952	0.555
Snow	-1.036	0.214	-1.470	-1.031	-0.628	-1.022
flat	-1.832	1.071	-3.811	-1.877	0.399	-1.970
summit	1.217	0.930	-0.444	1.158	3.209	1.036
ridge	0.442	0.463	-0.445	0.434	1.373	0.419
shoulder	0.000	31.623	-62.086	-0.001	62.034	0.000
spur	0.551	0.326	-0.083	0.548	1.197	0.544
hollow	0.136	0.423	-0.671	0.128	0.993	0.111
footslope	1.325	1.625	-1.423	1.164	4.928	0.817
valley	0.035	0.520	-0.954	0.023	1.091	0.000
depression	0.000	31.623	-62.086	-0.001	62.034	0.000
Elevation	-0.161	0.213	-0.585	-0.160	0.254	-0.157
Two-scale spatial model						
(Intercept)	1.184	0.153	0.888	1.181	1.500	1.175
Easting	1.701	1.856	-1.962	1.690	5.416	1.666
Northing	-0.626	0.331	-1.271	-0.631	0.054	-0.639
Two-scale spatial model and elevation						
(Intercept)	1.140	0.101	0.938	1.141	1.335	1.145
Easting	1.249	1.402	-1.483	1.239	4.030	1.217
Northing	-0.733	0.215	-1.165	-0.731	-0.315	-0.725
Elevation	-0.368	0.198	-0.762	-0.367	0.019	-0.366
Fixed effects model						
(Intercept)	2.184	0.183	1.840	2.178	2.559	2.167
Easting	-2.154	1.408	-4.938	-2.148	0.594	-2.137
Northing	-0.173	0.152	-0.473	-0.173	0.123	-0.172
Precipitation	0.191	0.151	-0.102	0.191	0.489	0.189
Snow	-0.730	0.168	-1.069	-0.727	-0.408	-0.721
flat	-2.058	0.936	-3.670	-2.142	0.000	-2.318
summit	0.305	0.854	-1.154	0.225	2.189	0.055
ridge	0.632	0.432	-0.180	0.618	1.521	0.591
shoulder	0.000	31.623	-62.086	-0.001	62.034	0.000
spur	0.383	0.300	-0.194	0.379	0.983	0.371
hollow	0.168	0.385	-0.549	0.153	0.965	0.125
footslope	-0.618	1.619	-3.247	-0.821	3.056	-1.281
valley	-0.315	0.471	-1.181	-0.336	0.669	-0.379
depression	0.000	31.623	-62.086	-0.001	62.034	0.000
Elevation	-0.343	0.147	-0.639	-0.340	-0.062	-0.335
Fixed Effects Parasite Survival Model						
(Intercept)	2.267	0.172	1.945	2.262	2.620	2.251
Precipitation	0.406	0.114	0.186	0.404	0.634	0.402
Snow	-0.733	0.137	-1.008	-0.730	-0.470	-0.726
flat	-1.980	0.922	-3.558	-2.066	0.054	-2.248
summit	0.349	0.858	-1.115	0.268	2.244	0.096
ridge	0.656	0.400	-0.087	0.640	1.487	0.609
shoulder	0.000	31.623	-62.086	-0.001	62.034	0.000
spur	0.410	0.285	-0.137	0.406	0.980	0.398

Table 3: Fixed effect parameter estimates and distribution for *F. magna (continued)*

variable	mean	sd	0.025quant	0.5quant	0.975quant	mode
hollow	0.284	0.378	-0.417	0.269	1.070	0.239
footslope	-0.340	1.622	-2.969	-0.545	3.342	-1.011
valley	-0.218	0.453	-1.043	-0.242	0.738	-0.289
depression	0.000	31.623	-62.086	-0.001	62.034	0.000

Table 4: Fixed effect parameter estimates and distribution for *P. tenuis*

variable	mean	sd	0.025quant	0.5quant	0.975quant	mode
Null Model						
(Intercept)	3.163	0.141	2.897	3.160	3.452	3.152
Full model						
(Intercept)	0.646	0.173	0.299	0.649	0.978	0.656
Easting	-3.802	2.021	-7.848	-3.778	0.110	-3.732
Northing	-0.413	0.297	-0.999	-0.413	0.170	-0.412
Precipitation	0.032	0.254	-0.455	0.028	0.541	0.021
Snow	-0.100	0.251	-0.610	-0.094	0.377	-0.082
flat	2.542	1.309	0.219	2.453	5.349	2.267
summit	0.596	1.212	-1.548	0.510	3.212	0.332
ridge	0.544	0.622	-0.649	0.534	1.798	0.514
shoulder	0.000	31.623	-62.086	-0.001	62.034	0.000
spur	1.247	0.415	0.439	1.244	2.067	1.239
hollow	0.996	0.556	-0.060	0.984	2.124	0.959
footslope	3.462	2.058	0.041	3.239	8.063	2.747
valley	-0.134	0.629	-1.322	-0.151	1.151	-0.184
depression	0.000	31.623	-62.086	-0.001	62.034	0.000
Elevation	-0.891	0.251	-1.385	-0.892	-0.398	-0.892
Two-scale spatial model						
(Intercept)	1.073	0.200	0.673	1.073	1.468	1.074
Easting	-1.684	2.378	-6.408	-1.679	3.002	-1.671
Northing	-0.053	0.423	-0.862	-0.063	0.816	-0.082
Two-scale spatial model and elevation						
(Intercept)	1.010	0.135	0.736	1.014	1.265	1.023
Easting	-4.127	1.762	-7.596	-4.128	-0.661	-4.130
Northing	-0.309	0.245	-0.797	-0.307	0.171	-0.304
Elevation	-1.048	0.227	-1.497	-1.047	-0.603	-1.045
Fixed effects model						
(Intercept)	2.053	0.212	1.656	2.045	2.491	2.031
Easting	-4.080	1.336	-6.730	-4.071	-1.481	-4.054
Northing	-0.200	0.187	-0.565	-0.200	0.167	-0.201
Precipitation	0.176	0.231	-0.272	0.174	0.634	0.170
Snow	-0.168	0.190	-0.546	-0.166	0.200	-0.162
flat	1.091	1.084	-0.729	0.979	3.504	0.738
summit	0.071	1.079	-1.768	-0.033	2.456	-0.252
ridge	0.702	0.481	-0.184	0.681	1.707	0.639
shoulder	0.000	31.623	-62.086	-0.001	62.034	0.000
spur	1.204	0.358	0.519	1.198	1.927	1.186
hollow	0.405	0.463	-0.448	0.385	1.371	0.345

Table 4: Fixed effect parameter estimates and distribution for *P. tenuis (continued)*

variable	mean	sd	0.025quant	0.5quant	0.975quant	mode
footslope	2.225	1.922	-0.851	1.970	6.613	1.376
valley	-0.228	0.555	-1.232	-0.259	0.948	-0.321
depression	0.000	31.623	-62.086	-0.001	62.034	0.000
Elevation	-0.869	0.202	-1.279	-0.865	-0.486	-0.855
Fixed Effects Parasite Survival Model						
(Intercept)	2.550	0.216	2.148	2.542	2.999	2.526
Precipitation	0.321	0.194	-0.056	0.320	0.706	0.317
Snow	-0.433	0.190	-0.807	-0.433	-0.061	-0.432
flat	0.830	1.129	-1.056	0.710	3.350	0.449
summit	-0.956	1.088	-2.784	-1.069	1.465	-1.311
ridge	0.445	0.494	-0.460	0.422	1.482	0.374
shoulder	0.000	31.623	-62.086	-0.001	62.034	0.000
spur	1.143	0.369	0.439	1.135	1.888	1.121
hollow	0.868	0.474	0.000	0.845	1.861	0.800
footslope	2.610	1.996	-0.566	2.339	7.175	1.704
valley	-0.390	0.563	-1.399	-0.425	0.813	-0.496
depression	0.000	31.623	-62.086	-0.001	62.034	0.000

Table 5: Random effect parameter estimates and distribution for *F. magna*

variable	mean	sd	0.025quant	0.5quant	0.975quant	mode
Null Model						
Nbinomial disp. par.	0.122	0.008	0.106	0.121	0.139	0.121
Full model						
Nbinomial disp. par.	0.170	0.015	0.142	0.170	0.201	0.169
Range for i	675.719	393.696	174.797	591.888	1689.579	430.606
Stdev for i	3.829	1.941	1.456	3.371	8.845	2.677
Two-scale spatial model						
Nbinomial disp. par.	0.157	0.013	0.131	0.157	0.183	0.158
Range for i	8822.205	6098.497	1930.233	7312.316	24616.287	4794.180
Stdev for i	1.365	0.285	0.827	1.364	1.924	1.379
Two-scale spatial model and elevation						
Nbinomial disp. par.	0.154	0.014	0.128	0.153	0.182	0.153
Range for i	762.009	771.156	106.883	535.157	2785.808	271.417
Stdev for i	4.462	3.808	0.754	3.401	14.466	1.923
Fixed effects model						
Nbinomial disp. par.	0.133	0.009	0.115	0.133	0.152	0.132
Fixed Effects Parasite Survival Model						
Nbinomial disp. par.	0.131	0.009	0.114	0.131	0.150	0.130

Table 6: Random effect parameter estimates and distribution for *P. tenuis*

variable	mean	sd	0.025quant	0.5quant	0.975quant	mode
Null Model						

Table 6: Random effect parameter estimates and distribution for *P. tenuis (continued)*

variable	mean	sd	0.025quant	0.5quant	0.975quant	mode
Nbinomial disp. par.	0.081	0.006	0.070	0.081	0.093	0.081
Full model						
Nbinomial disp. par.	0.111	0.010	0.092	0.110	0.132	0.110
Range for i	508.951	311.124	160.420	429.334	1343.793	318.308
Stdev for i	5.303	2.658	1.678	4.797	12.159	3.833
Two-scale spatial model						
Nbinomial disp. par.	0.111	0.010	0.093	0.111	0.131	0.110
Range for i	8705.474	4450.205	2871.060	7799.328	19903.368	6169.912
Stdev for i	1.892	0.397	1.297	1.827	2.838	1.688
Two-scale spatial model and elevation						
Nbinomial disp. par.	0.106	0.009	0.089	0.106	0.126	0.106
Range for i	585.296	394.178	169.375	478.445	1659.697	342.033
Stdev for i	4.439	2.257	1.315	4.029	9.984	3.166
Fixed effects model						
Nbinomial disp. par.	0.093	0.007	0.080	0.092	0.107	0.092
Fixed Effects Parasite Survival Model						
Nbinomial disp. par.	0.084	0.006	0.073	0.084	0.097	0.084